Reconciling the bulk metallic and surface insulating state in 1T-TaSe$_2$

Wenhao Zhang [1], Zongxiu Wu,[1] Kunliang Bu,[1] Ying Fei,[1] Yuan Zheng,[1] Jingjing Gao,[2,3] Xuan Luo,[2] Zheng Liu [4],
Yu-Ping Sun,[2,5,6] and Yi Yin [1,6,*]

[1]*Zhejiang Province Key Laboratory of Quantum Technology and Devices, Department of Physics,
Zhejiang University, Hangzhou 310027, China*
[2]*Key Laboratory of Materials Physics, Institute of Solid State Physics, Chinese Academy of Sciences, Hefei 230031, China*
[3]*Science Island Branch of Graduate School, University of Science and Technology of China, Hefei 230026, China*
[4]*Institute for Advanced Study, Tsinghua University, Beijing 100084, China*
[5]*High Magnetic Field Laboratory, Chinese Academy of Sciences, Hefei 230031, China*
[6]*Collaborative Innovation Center of Advanced Microstructures, Nanjing University, Nanjing 210093, China*

The origin of different electronic states of 1T-TaS$_2$ and 1T-TaSe$_2$ remains controversial due to the complicated correlated electronic properties. We apply scanning tunneling microscopy to study the electronic state of bulk 1T-TaSe$_2$. Both insulating and metallic states are identified in different areas of the same sample. The insulating state is similar to that in 1T-TaS$_2$, concerning both the dI/dV spectrum and the orbital texture. With detailed investigations in single-step areas, the electronic state measured on the upper-layer surface is found to be associated with different stacking orders and the lower layer's electronic state. The insulating state is most possibly a single-layer property, perturbed to a metallic state by particular stacking orders. Both the metallic and large-gap insulating spectra, together with their corresponding stacking orders, are stable states in 1T-TaSe$_2$. The connected metallic areas lead to the metallic transport behavior. We then reconcile the bulk metallic and surface insulating state in 1T-TaSe$_2$. The rich phenomena in 1T-TaSe$_2$ deepen our understanding of the correlated electronic state in bulk 1T-TaSe$_2$ and 1T-TaS$_2$.

I. INTRODUCTION

Layered transition metal dichalcogenides (TMDs) 1T-TaS$_2$ and 1T-TaSe$_2$ are two widely studied charge density wave (CDW) materials in the past few decades [1–10]. Both materials are at a commensurate CDW (CCDW) phase with a $\sqrt{13} \times \sqrt{13}$ reconstruction at low temperature. A single unpaired electron exists in each Star of David (SD), the basic element of the CCDW superlattice, resulting in a half-filled system. The electron-electron correlation can split the half-filled band to the lower and upper Hubbard band (LHB and UHB) with an insulating gap, called the Mott insulator [11]. In the bulk 1T-TaS$_2$, different experimental techniques confirm the insulating gap around the Fermi level, consistent with the transport result in 1T-TaS$_2$ [5–7]. The insulating gap nature of 1T-TaS$_2$ is still under debate [12–21], and is comprehensively studied in our other work [22].

For the bulk 1T-TaSe$_2$, the electronic state measured with different techniques is more complicated [23–26]. Both scanning tunneling microscopy (STM) and angle-resolved photoemission spectroscopy (ARPES) have detected an insulating state on the exposed surface [25,26]. However, the resistivity measurement shows a metallic behavior in the CCDW phase, also referred to as a bulk metallic state. The bulk metallic state and the surface insulating state have

to be reconciled in the same material, which is still far from a complete understanding. On the other hand, Se atoms in 1T-TaSe$_2$ share the same valence as S atoms in 1T-TaS$_2$ [27,28]. Whether the surface insulating state in 1T-TaSe$_2$ is similar to the correlation-induced state in 1T-TaS$_2$ needs to be clarified. The insulating state in the single-layer film of 1T-TaSe$_2$/TaS$_2$, grown by molecular beam epitaxy (MBE), makes the problem more complicated and fascinating [29,30].

Here we perform a detailed STM experiment to explore the electronic state of pristine 1T-TaSe$_2$ at low temperature. We find both metallic and insulating states frequently on the exposed surface of 1T-TaSe$_2$. The insulating spectrum in 1T-TaSe$_2$ is very similar to that in 1T-TaS$_2$, from the dI/dV spectrum to the spatial orbital texture. With multistep cleaved surfaces, we measure and obtain three different types of dI/dV spectra, including the large-gap, small-gap, and metallic spectra. The discrepancy of different electronic states in 1T-TaSe$_2$ is found to be associated with different stacking orders.

To infer the intrinsic stacking-order results in the bulk material, we focus on the flat single-step area and extend the measurement to areas away from the step edge. Both the large-gap insulating state and the metallic state are found to be a bulk property, while the small-gap spectrum only exists within a small area around the step edge. When the lower layer is metallic or insulating, we conclude the correspondence between the stacking order and the upper-layer electronic state, and list the number of occurrences of different situations. With
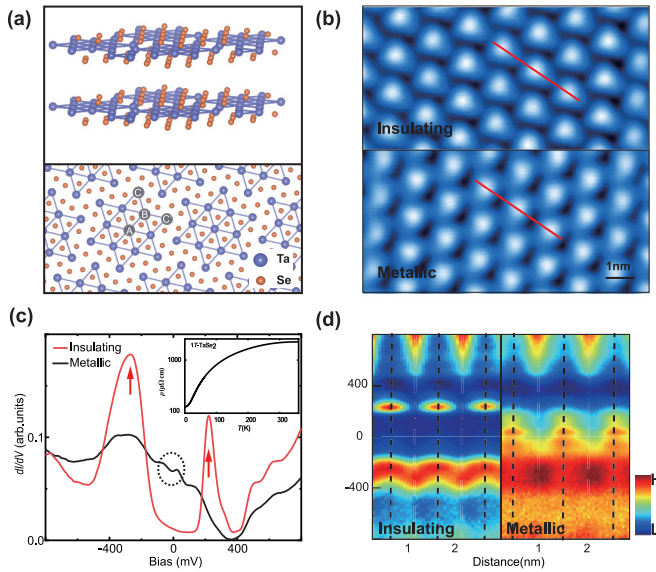
*yiyin@zju.edu.cn

035110-1

FIG. 1. Overview of structural and electronic properties of $1T$-TaSe$_2$. (a) Crystal structure of $1T$-TaSe$_2$. The side-view sketch is shown in the upper panel. The Star of David (SD) is formed by 13 Ta atoms in the CCDW phase, with the top-view sketch shown in the lower panel. Different Ta atoms are labeled by A, B, C, and C'. (b) Two 10×5 nm^2 topographies taken in the area of insulating (upper panel) and metallic (lower panel) state. (c) Typical dI/dV spectra taken in the area of insulating and metallic state (setup condition: $V_b = -600$ mV, $I_s = 500$ pA). The inset shows resistivity of bulk $1T$-TaSe$_2$ at the range of 2–360 K, exhibiting a metallic behavior at low temperature. (d) Two line-cut maps crossing three SDs along the red lines in (b). The periodic dI/dV evolution is displayed on the horizontal direction, in the bias voltage range of $[-800, 800]$ mV.

the large-gap insulating state most possibly the single-layer property of $1T$-TaSe$_2$, the metallic state could originate from the stacking-order-induced interlayer coupling and perturbation to the insulating state. The frequent appearance of the metallic state in $1T$-TaSe$_2$ leads to the macroscopic metallic transport results. The main difference between $1T$-TaS$_2$ and $1T$-TaSe$_2$ is that this perturbed metallic state is energetically stable in $1T$-TaSe$_2$ but not stable in $1T$-TaS$_2$. It requires a further theoretical study to explore how the stacking order induces this perturbation and the different stability of this metallic state in the two materials.

II. EXPERIMENT AND RESULTS

High-quality single crystal $1T$-TaSe$_2$ was grown with the iodine transport agent. In the STM experiment, $1T$-TaSe$_2$ were cleaved *in situ* in an ultrahigh-vacuum chamber (base pressure 4×10^{-11} mbar) at liquid nitrogen temperature and transferred to the STM head immediately. Topographies in this paper were collected with a bias voltage -600 mV and set-point current 500 pA at liquid nitrogen temperature (~ 77 K). The differential conductance dI/dV spectra were acquired by the standard lock-in technique, with a voltage modulation of 10 mV at 1213.7 Hz frequency.

Bulk single crystal $1T$-TaSe$_2$ has a CdI$_2$-type layered structure [upper panel of Fig. 1(a)]. In each unit structure,

the Ta atomic layer is sandwiched between two Se atomic layers, and the Ta atoms form a triangular lattice in the plane. In the CCDW phase, every 13 Ta atoms are regrouped into a cluster called the Star of David (SD), and the SDs form an enlarged triangular superlattice [lower panel in Fig. 1(a)]. The center and nearest Ta atoms are labeled by A and B, respectively, while the inequivalent next-nearest Ta atoms are labeled by C and C'. The electronic state is strongly modified by the CCDW phase. The bands from Ta atoms are folded into three subbands with two filled and one half filled [23]. In the bulk $1T$-TaS$_2$, the half-filled band is split into the LHB and UHB with a Mott insulating gap, consistent with the insulating state in the resistivity measurement. In contrast, the resistivity measurement of $1T$-TaSe$_2$ [Fig. 1(c) inset] shows a metallic state at low temperature [1–3]. The discrepancy of resistivity results of $1T$-TaS$_2$ and $1T$-TaSe$_2$ has been explained by the different p-derived valence bands of S and Se [31–35]. However, previous ARPES and STM experiments on bulk $1T$-TaSe$_2$ also observed that a surface metallic to Mott insulating phase transition occurs when the temperature is reduced to 260 K [25,26]. The reason for the coexistence of the bulk metallic and surface insulating states remains unresolved in $1T$-TaSe$_2$.

In our STM experiment, the measurement temperature (≈ 77 K) is far below the CCDW transition temperature. Insulating and metallic dI/dV spectra both exist in different areas of each sample we measured. Figure 1(b) shows two representative topographies with different electronic states. They share the same triangular SD superlattice array, with each bright spot corresponding to one SD. Figure 1(c) shows the typical insulating and metallic spectra measured at the center of one SD. The insulating dI/dV spectrum is very similar to the Mott insulating spectrum measured in bulk $1T$-TaS$_2$. The LHB and UHB peaks are located at -300 and 230 mV. The gap size is around 530 mV, about 100 mV larger than that of bulk $1T$-TaS$_2$ [35–37]. The CDW valley roughly at 400 mV shows an approximate zero value, suggesting a strong CDW modulation in $1T$-TaSe$_2$ [28]. The metallic dI/dV spectrum displays a rough linear decay of density of states (DOS) around the Fermi energy (zero bias). A weak dip feature appears around the zero bias. The deep valley at 400 mV coincides with the CDW valley in the insulating dI/dV spectrum.

To show the spatial homogeneity, we present the line-cut maps for both the insulating and metallic states. In Fig. 1(d), the horizontal axis is the position along the two red lines crossing three SDs in Fig. 1(b), and the vertical axis is the STM bias ranging from -800 to 800 mV. For the insulating spectra, the LHB and UHB peaks are evident at SD centers, resulting in a periodic intensity variation along the line. The CDW feature above 400 mV also shows an apparent periodic variation, but with maximum peaks shifting by half the period. This phenomenon is similar to that in $1T$-TaS$_2$ [35,36]. The Hubbard bands originate from the central Ta orbital, with LHB and UHB peaks showing maximum values at SD centers. The CDW bands are from the surrounding Ta orbital, with CDW peaks showing maximum values at SD rims. In the line-cut map of metallic spectra, the zero-bias dip also shows a periodic variation, and the maximum values are located at SD centers. We expect that the two peaks of the zero-bias dip in the metallic spectrum are also related to the central Ta orbital.
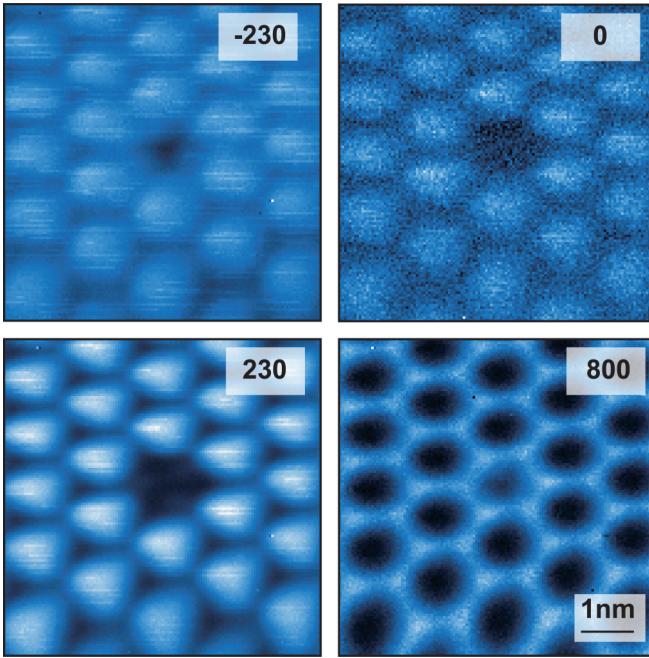
FIG. 2. The dI/dV maps at several selected energies $(-230, 0, 230, 800$ mV) for a 6×6 nm^2 area with insulating state. A defective SD exists in the middle of this area.

Figure 2 displays the differential conductance dI/dV maps at several selected energies for a 6×6 nm^2 area with insulating state. A special point defect exists at one SD in the middle of the frame, which is identified with a central Ta vacancy in $1T$-TaS$_2$ [22]. The dI/dV maps reveal more spatial characteristics than the line-cut map crossing SDs. With the bias voltage at -230 mV and 230 mV, these two dI/dV maps are close to the LHB and UHB, respectively. Both maps display a triangular lattice pattern with the bright spots positioned at SD centers, consistent with that the Hubbard band mainly originates from the central Ta orbital. When moving to the lower energy or higher energy, the dI/dV maps reveal a honeycomb orbital texture (e.g., in the map at 800 mV), consistent with that the CDW bands are from the surrounding Ta orbitals. The energy-dependent orbital texture for the insulating state is similar to that in the bulk $1T$-TaS$_2$ [35]. The single-layer MBE-grown $1T$-TaSe$_2$ shows a slightly different energy-dependent orbital texture despite the similar insulating spectrum [29,30]. The similar insulating spectra in the single-layer and bulk samples suggest that the insulating state is most likely an intrinsic single-layer property.

The reason for the different electronic states in different regions is still a mystery. Stacking order has been taken into account in some recent research works [12–21]. In our other work [22], stacking order has been studied in detail in $1T$-TaS$_2$. We apply a similar procedure to study the step areas on cleaved bulk $1T$-TaSe$_2$ [22]. Figure 3(a) shows a special large-area topography with multistep environment, taken on the exposed surface of $1T$-TaSe$_2$. A schematic side view of this multistep area is shown in Fig. 3(b), which is derived from the height profiles in topography. As shown in Fig. 3(c), the dI/dV spectra measured on different step planes exhibit different electronic states.
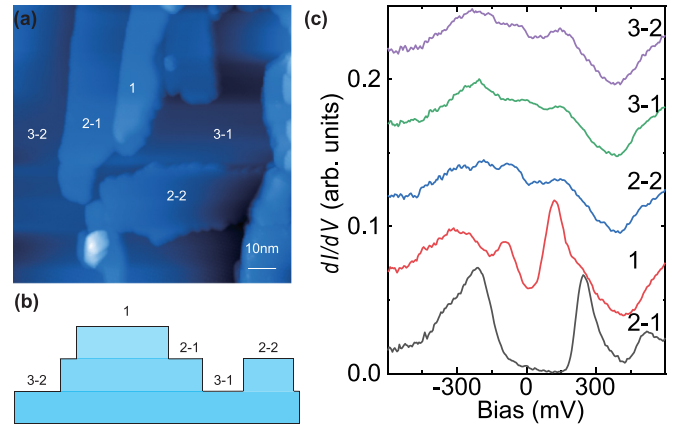

FIG. 3. Topography and corresponding electronic spectra in a multistep area. (a) A 100×100 nm^2 topography, with a schematic side view shown in (b). (c) Typical dI/dV spectra on different regions in (a). The spectrum in regions 3-1, 3-2, and 2-2 shows a normal metallic state of $1T$-TaSe$_2$, while the spectra in regions 2-1 and 1 show a large-gap state and a small-gap state, respectively.

For the area in Fig. 3(a), the dI/dV spectrum on the bottom layer (region 3-1 and region 3-2) is a metallic one similar to that in Fig. 1(c). On top of this layer, the dI/dV spectra exhibit different electronic states, insulating in region 2-1 and metallic in region 2-2. Different electronic states in the same plane (regions 2-1 and 2-2) imply that different stacking orders exist between the same two layers. Furthermore, the dI/dV spectrum in region 1 has a reduced gap with peaks at -70 and 140 mV. Although the zero-bias conductance of this type of spectrum is enhanced to a significant value, the curve shape is consistent with the small-gap spectrum in $1T$-TaS$_2$ [22]. This phenomenon reminds us of the similar three types of spectra in the stacking order study in $1T$-TaS$_2$ [22].

To study the stacking order, we focus on the flat single-step area which renders a determination of the relative displacement of SD superlattices in the upper and lower layers. The method is similar to that in our other work [22]. The single-step area also enables us to extend the measurement away from the step edge to check whether the result is more related to the bulk property. In multiple experiments, we only occasionally observe the small-gap spectrum, which also exists within a small area around the step edge or in a small island area [Fig. 3(a)]. Then we mainly concentrate attention on the large-gap and metallic spectra, which are more related to the intrinsic property of the bulk material. For the following shown examples, they are selected from multiple measurements on different samples.

We first consider the situation with a metallic spectrum on the lower layer. Figures 4(a) and 4(b) show two single-step area topographies, which include triangular SD superlattices in both the lower layer and the bright upper layer. The spectra measured on the lower and upper layers are shown in Figs. 4(c) and 4(d). On the upper layer, the electronic state shows a metallic spectrum in Fig. 4(c). The metallic dI/dV spectra of the two layers are basically the same with a slight difference near the Fermi level. The corresponding stacking order is the AC stacking, which means that the SD center of the upper layer is vertically aligned with the outer-corner
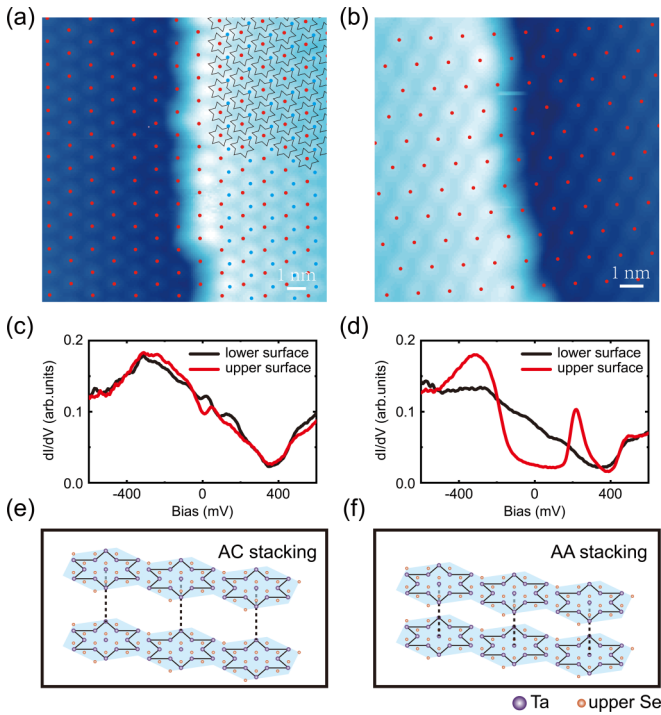
FIG. 4. The stacking orders and corresponding dI/dV spectra with a lower-layer metallic spectrum. (a) and (b) STM topographies of a single-step area. The red (blue) dots mark SD centers in the lower (upper) layer. The SD centers in the upper layer are aligned with the SD outer-corner sites (*AC*-stacking order), or center sites (*AA*-stacking order) in the lower layer. (c) and (d) The red and black lines are the dI/dV spectra on the upper and lower layers in (a) and (b). (e) and (f) The schematic diagrams of the stacking orders in (a) and (b).

site of SD in the underlying layer as shown in Fig. 4(e). The metallic-metallic steps are frequently observed during our experiments. Another commonly observed case is the insulating upper layer observed with *AA* stacking [Figs. 4(d) and 4(f)]. It is worth mentioning that although the small-gap spectrum is rarely observed above the metallic layer, the corresponding stacking order is the *AB* stacking. Up to our current experiments, the surface electronic states above a metallic layer all show a one-to-one correspondence with stacking orders.

We further consider the situation with an insulating spectrum on the lower layer. The insulating-insulating steps, which are most frequently observed in $1T$-TaS$_2$, are also commonly seen in $1T$-TaSe$_2$. Differently from $1T$-TaS$_2$, the *AA* stacking of the insulating-insulating step only occasionally appears in $1T$-TaSe$_2$. The dominate stacking order is the *AC* stacking [Figs. 5(a), 5(d), and 5(g)]. Figures 5(b) and 5(c) show two single-step area topographies, with the metallic spectra measured on the upper layers [Figs. 5(e) and 5(f)]. After carefully determining the relative shift of SD superlattices, the metallic layer in Fig. 5(b) corresponds to the *AC'* stacking, which is inequivalent to the *AC* stacking in Fig. 5(a). Figure 5(c) corresponds to the *AB*-stacking order. With multiple measurements, we find that these three cases are all frequent and constantly reproducible.

TABLE I. Summary of different stacking orders observed during the experiments.

Lower-layer electronic state	Upper-layer electronic state	Stacking order	Number
Metallic	Metallic	*AC*	6
	Large-gap insulating	*AA*	4
Large-gap insulating	Large-gap insulating	*AC*	7
		AA	1
	Metallic	*AC'*	5
		AB	5

All different stacking orders and the corresponding electronic states of upper and lower layers are summarized in Table I. As the table shows, the stacking order shows one-to-one correspondence with the upper-layer electronic state, when the lower layer is metallic. When the lower layer is insulating, two different stacking orders can lead to the same upper-layer electronic state. A similar case has happened in $1T$-TaS$_2$ [22], in which both *AA* and *AC* stacking lead to the insulating-insulating step. Considering the single-layer property of the large-gap spectrum, both *AA* and *AC* stacking may lead to a negligible interlayer coupling. In contrast, the *AC'* and *AC* stacking result in a similar perturbed and metallic upper-layer spectrum. The upper-layer spectrum is not only related to the stacking order, but also to the spectrum of the lower layer. The *AC*-stacking order could correspond to a metallic spectrum in Fig. 4(a) but an insulating spectrum in Fig. 5(a).

There are long-standing puzzles about the insulating state in bulk $1T$-TaS$_2$ and $1T$-TaSe$_2$. According to the first-principles calculation, there is a conducting band along the ΓA direction, which leads to a metallic state near the Fermi level. However, the large insulating gap near the Fermi level has been identified by different experimental methods. Recently, some experiments reveal possible double-layer stacking in $1T$-TaS$_2$, which conjures up a band insulator scenario [18–20]. In our comprehensive results, the *AC* stacking in Fig. 5(a) corresponds to two large-gap spectra on both the upper and lower terraces, which dispels that the large gap is from the unit-cell doubling of two *AA*-stacked layers [18–20]. In fact, different stacking orders appear randomly in our samples. The upper-layer electronic state is determined by the stacking orders and the electronic state of the adjacent underlying layer. The large-gap spectrum is most possibly the intrinsic property of a single-layer $1T$-TaSe$_2$, similar to that of the MBE-grown film of $1T$-TaSe$_2$. The metallic spectrum is not intrinsic in the single-layer $1T$-TaSe$_2$, but a modulated spectrum induced by particular stacking orders.

The metallic spectrum in $1T$-TaSe$_2$ shows a rough linear DOS near the Fermi level, different from the V-shaped metallic spectrum in $1T$-TaS$_2$. The difference is possibly related to the different valence band of S and Se. The Se atom valence band has a higher energy level than that of the S atom, making it easier for the band to hybridize with the d band of Ta atoms. On top of the insulating layer, a metallic layer can be induced by the *AC'*-stacking and *AB*-stacking orders. Above the metallic layer, the *AC* stacking leads to the
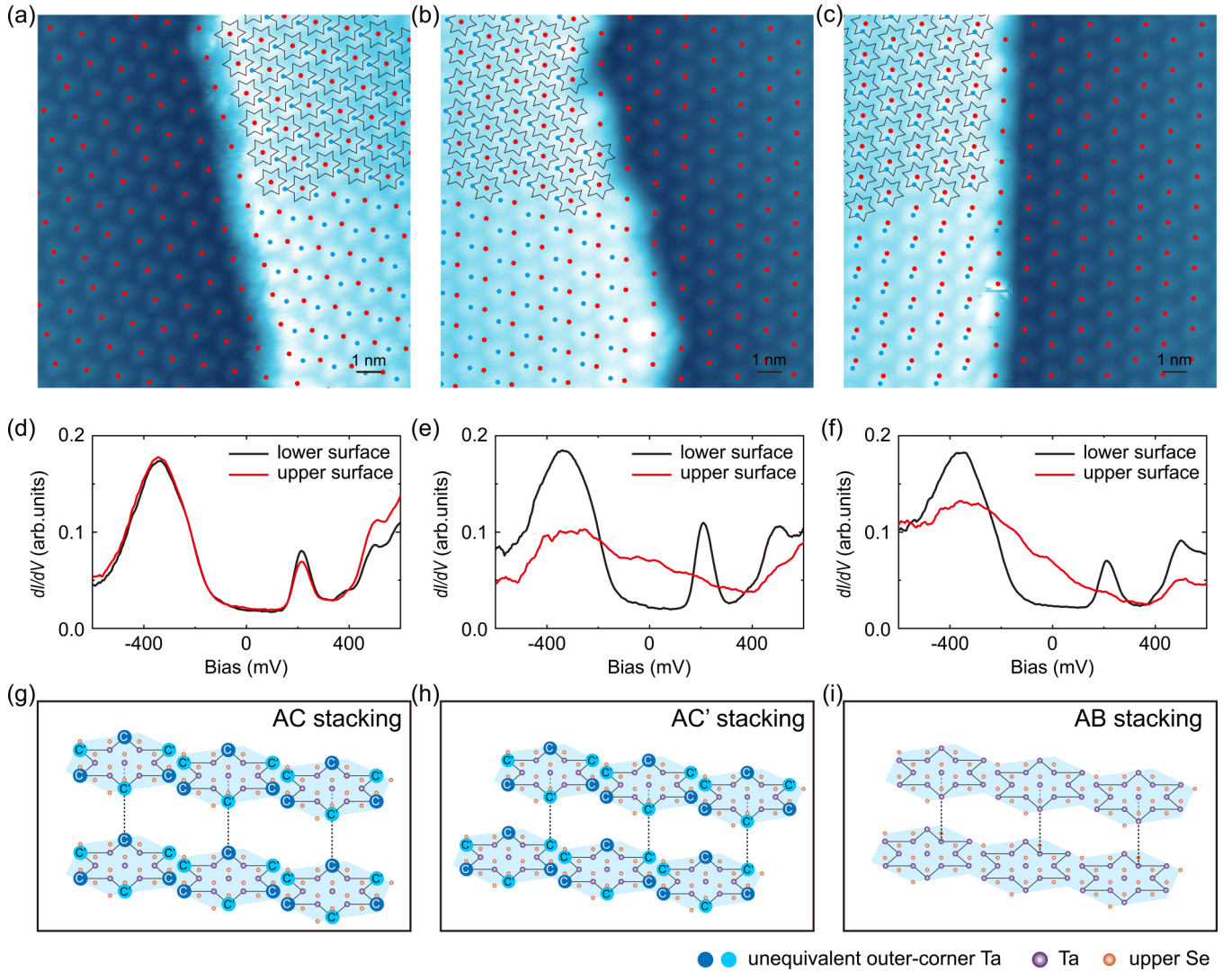
FIG. 5. The stacking orders and corresponding dI/dV spectra with a lower-layer insulating spectrum. (a) STM topography of a single-step area. The red (blue) dots mark SD centers in the lower (upper) layer. The SD centers in the upper layer are aligned with the SD outer-corner sites in the lower layer, or in the AC-stacking order. (b), (c) STM topographies of two other single-step areas, in the AC'-stacking or AB-stacking order as shown in the superimposed SD centers. (d)–(f) The red and black lines are the dI/dV spectra on the upper and lower layers in (a)–(c). (h), (i) The schematic diagrams of the stacking orders in (a)–(c).

metallic upper-layer state. When the electron correlation is disturbed, the strong charge transfer between Ta and Se atoms is possibly dominant, leading to the linear DOS decay near the Fermi level. The difference between Se and S bands may also make the metallic perturbed state more stable in terms of energy, while the theoretical explanation is beyond our current capability and needs further investigations.

In $1T$-TaSe$_2$, both the metallic and large-gap insulating states can extend all the way at the step edge, although only the large-gap spectrum can extend all the way in $1T$-TaS$_2$. The difference is consistent with that both insulating state and metallic state can appear at different regions in the same sample in $1T$-TaSe$_2$, while only the insulating state dominates in $1T$-TaS$_2$. Please note that although we can only measure the spectrum on exposed terraced areas, the collected information helps to predict the electronic state layer-by-layer when we know the state of the underlying layer and the stacking order.

III. CONCLUSION

Combining all above information, we demonstrate that the stacking order plays a crucial role in determining the electronic state in bulk $1T$-TaSe$_2$. The main difference between bulk $1T$-TaS$_2$ and $1T$-TaSe$_2$ is that the large-gap insulating spectrum dominates in $1T$-TaS$_2$. In contrast, many different stacking orders can induce both insulating and metallic states depending on the electronic states of the underlying layer in $1T$-TaSe$_2$. A large enough ratio of metallic state can always yield a metallic state in the macroscopic transport measurement.

In pristine $1T$-TaSe$_2$, the large-gap insulating state mainly reflects the intrinsic single-layer Mott gap, while some spectral details like the nonzero conductance around the Fermi energy and the slope from LHB to zero bias position may be related to the interlayer effect along the c axis. In general, the interlayer coupling plays a stronger role in $1T$-TaSe$_2$ than

in $1T$-TaS$_2$. The extremely easy modulation of the electronic state can also make the MBE film slightly different from the insulating state in the bulk sample, possibly related to the substrate-induced effect or the particular growth condition. The Mott physics in TMD materials $1T$-TaSe$_2$ and $1T$-TaS$_2$ is proved to be exceptionally rich and deserves further exploration.

[1] J. A. Wilson, F. J. Di Salvo, and S. Mahajan, Charge-density waves and superlattices in the metallic layered transition metal dichalcogenides, Adv. Phys. **24**, 117 (1975).

[2] F. J. Di Salvo, J. A. Wilson, B. G. Bagley, and J. V. Waszczak, Effects of doping on charge-density waves in layer compounds, Phys. Rev. B **12**, 2220 (1975).

[3] P. Fazekas and E. Tosatti, Electrical, structural and magnetic properties of pure and doped $1T$-TaS$_2$, Philos. Mag. B **39**, 229 (1979).

[4] K. Rossnagel, On the origin of charge-density waves in select layered transition-metal dichalcogenides, J. Phys.: Condens. Matter **23**, 213001 (2011).

[5] J. J. Kim, W. Yamaguchi, T. Hasegawa, and K. Kitazawa, Observation of Mott Localization Gap Using Low Temperature Scanning Tunneling Spectroscopy in Commensurate $1T$-TaS$_2$, Phys. Rev. Lett. **73**, 2103 (1994).

[6] J. J. Kim, I. Ekvall, and H. Olin, Temperature-dependent scanning tunneling spectroscopy of $1T$-TaS$_2$, Phys. Rev. B **54**, 2244 (1996).

[7] N. V. Smith, S. D. Kevan, and F. J. DiSalvo, Band structures of the layer compounds $1T$-TaS$_2$ and $1H$-TaSe$_2$ in the presence of commensurate charge-density waves, J. Phys. C: Solid State Phys. **18**, 3175 (1985).

[8] B. Sipos, A. F. Kusmartseva, A. Akrap, H. Berger, L. Forró, and E. Tutiš, From Mott state to superconductivity in $1T$-TaS$_2$, Nat. Mater. **7**, 960 (2008).

[9] I. Lutsyk, M. Rogala, P. Dabrowski, P. Krukowski, P. J. Kowalczyk, A. Busiakiewicz, D. A. Kowalczyk, E. Lacinska, J. Binder, N. Olszowska, M. Kopciuszynski, K. Szalowski, M. Gmitra, R. Stepniewski, M. Jalochowski, J. J. Kolodziej, A. Wysmolek, and Z. Klusek, Electronic structure of commensurate, nearly commensurate, and incommensurate phases of $1T$-TaS$_2$ by angle-resolved photoelectron spectroscopy, scanning tunneling spectroscopy, and density functional theory, Phys. Rev. B **98**, 195425 (2018).

[10] E. Lahoud, O. N. Meetei, K. B. Chaska, A. Kanigel, and N. Trivedi, Emergence of a Novel Pseudogap Metallic State in a Disordered 2D Mott Insulator, Phys. Rev. Lett. **112**, 206402 (2014).

[11] N. F. Mott, Metal-insulator transition, Rev. Mod. Phys. **40**, 677 (1968).

[12] T. Ritschel, J. Trinckauf, K. Koepernik, B. Büchner, M. v. Zimmermann, H. Berger, Y. I. Joe, P. Abbamonte, and J. Geck, Orbital textures and charge density waves in transition metal dichalcogenides, Nat. Phys. **11**, 328 (2015).

[13] T. Ritschel, H. Berger, and J. Geck, Stacking-driven gap formation in layered $1T$-TaS$_2$, Phys. Rev. B **98**, 195134 (2018).

[14] S. H. Lee, J. S. Goh, and D. Cho, Origin of the Insulating Phase and First-Order Metal-Insulator Transition in $1T$-TaS$_2$, Phys. Rev. Lett. **122**, 106404 (2019).

[15] D. B. Shin, T.-D. Nicolas, J. Zhang, M. S. Okyay, A. Rubio, and N. Park, Identification of the Mott Insulating Charge Density Wave State in $1T$-TaS$_2$, Phys. Rev. Lett. **126**, 196406 (2021).

[16] L. Ma, C. Ye, Y. Yu, X. F. Lu, X. Niu, S. Kim, D. Feng, D. Tománek, Y. W. Son, X. H. Chen, and Y. B. Zhang, A metallic mosaic phase and the origin of Mott-insulating state in $1T$-TaS$_2$, Nat. Commun. **7**, 10956 (2016).

[17] D. Cho, S. Cheon, K. S. Kim, S. H. Lee, Y. H. Cho, S. W. Cheong, and H. W. Yeom, Nanoscale manipulation of the Mott insulating state coupled to charge order in $1T$-TaS$_2$, Nat. Commun. **7**, 10453 (2016).

[18] C. J. Butler, M. Yoshida, T. Hanaguri, and Y. Iwasa, Mottness versus unit-cell doubling as the driver of the insulating state in $1T$-TaS$_2$, Nat. Commun. **11**, 2477 (2020).

[19] C. J. Butler, M. Yoshida, T. Hanaguri, and Y. Iwasa, Doublonlike Excitations and Their Phononic Coupling in a Mott Charge-Density-Wave System, Phys. Rev. X **11**, 011059 (2021).

[20] J. Lee, K.-H. Jin, and H. W. Yeom, Distinguishing a Mott Insulator from a Trivial Insulator with Atomic Adsorbates, Phys. Rev. Lett. **126**, 196405 (2021).

[21] Y. D. Wang, W. L. Yao, Z. M. Xin, T. T. Han, Z. G. Wang, L. Chen, C. Cai, Y. Li, and Y. Zhang, Band insulator to Mott insulator transition in $1T$-TaS$_2$, Nat. Commun. **11**, 4215 (2020).

[22] Z. Wu, K. Bu, W. Zhang, Y. Fei, Y. Zheng, J. Gao, X. Luo, Z. Liu, Y.-P. Sun, and Y. Yin, Effect of stacking order on the electronic state of $1T$-TaS$_2$, Phys. Rev. B **105**, 035109 (2022).

[23] K. Horiba, K. Ono, J. H. Oh, T. Kihara, S. Nakazono, M. Oshima, O. Shiino, H. W. Yeom, A. Kakizaki, and Y. Aiura, Charge-density wave and three-dimensional Fermi surface in $1T$-TaSe$_2$ studied by photoemission spectroscopy, Phys. Rev. B **66**, 073106 (2002).

[24] J. J. Kim, W. Yamaguchi, T. Hasegawa, and K. Kitazawa, Site-specified tunneling spectroscopy of local density of states in the charge-density-wave state of $1T$-TaSe$_2$ at 77 K, Phys. Rev. B **50**, 4958(R) (1994).

[25] L. Perfetti, A. Georges, S. Florens, S. Biermann, S. Mitrovic, H. Berger, Y. Tomm, H. Höchst, and M. Grioni, Spectroscopic Signatures of a Bandwidth-Controlled Mott Transition at the Surface of 1*T*-TaSe$_2$, Phys. Rev. Lett. **90**, 166401 (2003).

[26] S. Colonna, F. Ronci, A. Cricenti, L. Perfetti, H. Berger, and M. Grioni, Mott Phase at the Surface of 1*T*-TaSe$_2$ Observed by Scanning Tunneling Microscopy, Phys. Rev. Lett. **94**, 036405 (2005).

[27] P. Darancet, A. J. Millis, and C. A. Marianetti, Three-dimensional metallic and two-dimensional insulating behavior in octahedral tantalum dichalcogenides, Phys. Rev. B **90**, 045134 (2014).

[28] Y. Z. Ge and A. Y. Liu, First-principles investigation of the charge-density-wave instability in 1*T*-TaSe$_2$, Phys. Rev. B **82**, 155133 (2010).

[29] Y. Chen, W. Ruan, M. Wu, S. Tang, H. Ryu, H. Z. Tsai, R. Lee, S. Kahn, F. Liou, C. Jia, Oliver R. Albertini, H. Xiong, Tao Jia, Z. Liu, J. A. Sobota, A. Y. Liu, J. E. Moore, Z. X. Shen, S. G. Louie, S. K. Mo *et al.*, Strong correlations and orbital texture in single-layer 1*T*-TaSe$_2$, Nat. Phys. **16**, 218 (2020).

[30] H. Lin, W. Huang, K. Zhao, S. Qiao, Z. Liu, J. Wu, X. Chen, and S. H. Ji, Scanning tunneling spectroscopic study of monolayer 1*T*-TaS$_2$ and 1*T*-TaSe$_2$, Nano Res. **13**, 133 (2020).

[31] F. Clerc, M. Bovet, H. Berger, L. Despont, C. Koitzsch, O. Gallus, L. Patthey, M. Shi, J. Krempasky, M. G. Garnier, and P. Aebi, Spin-orbit splitting in the valence bands of 1*T*-TaS$_2$ and 1*T*-TaSe$_2$, J. Phys.: Condens. Matter **16**, 3271 (2004).

[32] M. Bovet, D. Popović, F. Clerc, C. Koitzsch, U. Probst, E. Bucher, H. Berger, D. Naumović, and P. Aebi, Pseudogapped Fermi surfaces of 1*T*-TaS$_2$ and 1*T*-TaSe$_2$: A charge density wave effect, Phys. Rev. B **69**, 125117 (2004).

[33] Y. Liu, R. Ang, W. J. Lu, W. H. Song, L. J. Li, and Y. P. Sun, Superconductivity induced by Se-doping in layered charge-density-wave system 1*T*-TaS$_{2-x}$Se$_x$, Appl. Phys. Lett. **102**, 192602 (2013).

[34] R. Ang, Y. Miyata, E. Ieki, K. Nakayama, T. Sato, Y. Liu, W. J. Lu, Y. P. Sun, and T. Takahashi, Superconductivity and bandwidth-controlled Mott metal-insulator transition in 1*T*-TaS$_{2-x}$Se$_x$, Phys. Rev. B **88**, 115145 (2013).

[35] S. Qiao, X. T. Li, N. Z. Wang, W. Ruan, C. Ye, P. Cai, Z. Q. Hao, H. Yao, X. H. Chen, J. Wu, Y. Y. Wang, and Z. Liu, Mottness Collapse in 1*T*-TaS$_{2-x}$Se$_x$ Transition-Metal Dichalcogenide: An Interplay between Localized and Itinerant Orbitals, Phys. Rev. X **7**, 041054 (2017).

[36] D. Cho, Y. H. Cho, S. W. Cheong, K. S. Kim, and H. W. Yeom, Interplay of electron-electron and electron-phonon interactions in the low-temperature phase of 1*T*-TaS$_2$, Phys. Rev. B **92**, 085132 (2015).

[37] K. L. Bu, W. H. Zhang, Y. Fei, Z. X. Wu, Y. Zheng, J. J. Gao, X. Luo, Y. P. Sun, and Y. Yin, Possible strain induced Mott gap collapse in 1*T*-TaS$_2$, Commun. Phys. **2**, 146 (2019).